The 7th International Supercritical CO_2 Power Cycles Symposium
February 21, 2022 – February 24, 2022, San Antonio TX
Paper # 172

Mechanical degradation of Ferritic/Martensitic and Austenitic steels in CO_2 environment

Kyle A. Rozman
National Energy Technology Laboratory and Support Contractor
Albany, OR USA
kyle.rozman@netl.doe.gov

Richard P. Oleksak
National Energy Technology Laboratory and Support Contractor
Albany, OR USA
richard.oleksak@netl.doe.gov

Sajedur R. Akanda
Research Engineer
GE Research
Niskayuna, NY, USA
Sajedur.Akanda@gmail.com

Casey S. Carney
National Energy Technology Laboratory and Support Contractor
Albany, OR USA
casey.carney@netl.doe.gov

Ömer N. Doğan
Materials Research Engineer
National Energy Technology Laboratory
Albany, OR USA
omer.dogan@netl.doe.gov

Kyle Rozman is currently an employee of LRST as a contractor to the United States Department of Energy - National Energy Technology Laboratory in Albany, OR, where he has worked since 2017. Kyle received his Ph.D. from Oregon State University in Materials Science in 2014. Kyle's research interests include environmental effects on fatigue and fracture of metallic materials.

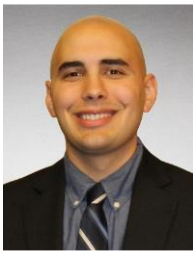

Richard Oleksak is an LRST Research Scientist working with the Structural Materials Team at NETL. He received his Ph.D. from Oregon State University in Chemical Engineering in 2015. His current research focuses on understanding the oxidation and corrosion behavior of structural alloys for next-generation power systems.

Sajedur Akanda is currently working as a research engineer at GE Research. He worked as a post- doctoral researcher at NETL from 2016 to 2020. He received his PhD in Mechanical Engineering from The Ohio State University in 2013. His research interest includes lifing and durability of barrier coatings and materials, materials fatigue, fracture, and mechanical degradation by CO_2 corrosive environments

Casey Carney received his B.S. in chemistry and engineering physics from Hope College. He received his Ph.D. in Chemical Engineering from the University of Colorado in 2005. He is currently an employee of LRST as a contractor to the United States Department of Energy - National Energy Technology Laboratory in Albany, OR, where he has worked since 2008. His recent research topics have included: oxy-combustion flame analysis, thermal decomposition kinetics, and materials performance in extreme combustion and supercritical CO2 environments.

Ömer Doğan is a Materials Research Engineer in the Structural Materials Team in the Research & Innovation Center at NETL. He received his Ph.D. from Case Western Reserve University in Materials Science & Engineering in 1990. Current research focuses on the evaluation and development of heat, corrosion, and wear resistant materials for applications in harsh environments.

Abstract

Determining the mechanical properties for materials in CO_2 environments is critical for structural alloys in supercritical CO_2 power cycle applications. Ferritic/Martensitic 9%Cr steels (P91 and MARBN) and austenitic 347H were tested to quantify the degradation in mechanical properties caused by CO_2. Room temperature tensile tests were performed on thick (2.5 mm) and thin (0.5 mm) specimens after exposure to direct fired CO_2 cycle conditions for 1000 hours. The thin and thick specimens of P91 experienced significant degradation in tensile properties during the exposure while only the thin specimens for austenitic alloy 347H experienced significant degradation. This was attributed to a change in oxidation behavior, where protective Cr-rich oxide scales formed on the thicker 347H specimens and non-protective Fe-rich oxide scales formed on the thinner specimens. Concurrent with the non-protective Fe-rich oxide layer, the thinner specimen of 347H also experienced extensive carburization.

Environmental creep tests were also performed in gaseous CO_2 at 650°C. Creep tests on MARBN alloy showed severe reduction in time to rupture relative to tests conducted in air. This was attributed to a an environmentally-assisted cracking mechanism. Creep tests on austenitic 347H are ongoing.

Introduction

Significant knowledge has been gained on engineering materials and oxidation in sCO_2 (supercritical carbon dioxide) power cycles which has been previously presented in this symposium. However, a knowledge gap remains as to the in-situ materials performance in CO_2. The oxidation response of martensitic 9%Cr steels in CO_2 is summarized in [1]. Briefly it was discovered that 9%Cr steels form duplex Fe-rich oxide scales which follow parabolic law oxidation kinetics. Further, the 9%Cr steels were susceptible to enhanced carburization because they are unable to form a protective Cr-rich oxide layer. For higher Cr (18-25%) austenitic steels, a Cr-rich oxide scale is usually formed in CO_2 environments. However, it has been found in CO_2 environments, the continuous Cr-rich oxide layer can be interrupted, temporarily forming Fe-rich oxides.

Some previous ex-situ experiments have shown little change to tensile mechanical properties after exposures to CO_2 [2-5]. However, for thin section samples Akanda et al. [6] found a significant loss of ductility for post-exposure tensile properties.

For in-situ testing, some studies are complicated with mixed results on austenitic stainless steels [7, 8]. Guo et al. [9] studied austenitic HP-Nb steel tubes (26%wt Cr, 35%wt Ni, Bal. Fe) in ethylene environments, which are similar to CO_2, and found severe carburization featuring both coarsened and interconnected the carbides, leading to an overall degradation in mechanical performance. Kim et al. [10], studied alloy 600 in a specially designed autoclave for creep testing alloys in sCO_2. Kim et al., found air and gaseous CO_2 creep lives overlapped while the creep life in sCO_2 was 2-3X shorter. Rozman et al. [11] creep tested a 9%Cr martensitic alloy in CO_2 environment and found a severe loss in creep life for the 9%Cr alloy creep tested in CO_2 as compared to testing in air.

This manuscript summarizes prior and ongoing work at NETL investigating the effects of CO_2 on the mechanical degradation of these engineering steels which are candidate materials for sCO_2 power cycles. This research includes ex-situ tensile testing of P91 and 347H steels after exposure to a CO_2-rich environment and environmental (in-situ) creep testing of a martensitic 9%Cr steel in CO_2. Environmental creep testing of alloy 347H is ongoing.

Materials and Experimental Methods

A commercial plate of P91 steel was purchased from Arcelormittal Plate LLC. The plate was normalized at 1038°C for ~4 h, then air cooled to room temperature and tempered at 788°C for ~1.5 h followed by air cooling to room temperature. The composition provided by the manufacturer is tabulated in Table 1.

A plate of commercial 347H was purchased from Outokumpu Stainless Plate LLC. The plate was annealed at 1065°C and then quenched by the manufacturer. The information on the 347H stainless steels is found in Table 1.

Table 1 Chemical compositions (wt.%) of P91 and 347H steels.

Metal	Cr	C	Mn	P	S	Cu	Si	Ni	Mo	Ti	Al	N	Fe
P91	8.37	0.09	0.45	0.01	0.004	0.09	0.33	0.09	0.90	0.002	0.007	0.045	Balance
347H	17.26	0.05	1.5	0.034	0.001	0.43	0.38	9.09	0.41	0.005	0.007	0.04	Balance
MARBN	9.08	0.15	0.51	-	-	0.03	0.24	0.18	0.10	-	-	0.02	Balance

The MARBN-type steel (MARtensitic steel with Boron and Nitrogen) used in this research was designed and manufactured at NETL using vacuum induction melting (VIM). The melt charge was made up of commercial high purity material in loose, as well as compacted, form to facilitate crucible loading and melting in the zirconia crucible. The liquid was brought to a temperature 50°C above the melting temperature (superheat) in a N_2 and Ar atmosphere. The molten alloy was poured into a 76 mm diameter graphite mold with zirconia mold wash coat to prevent excessive C pickup from the graphite mold. Following casting, slices were cut from the ingot for chemistry analysis using X-ray fluorescence (XRF) on a Rigaku ZSX Primus II system while C, N, O and S were determined by combustion analysis using LECO systems. The B fraction was analyzed using inductively coupled plasma (ICP) approach.

The ingot was then homogenized in a vacuum heat treatment furnace using a computationally optimized heat treatment schedule that yielded a predicted homogeneity of ±1% of nominal (or better) for each element [12]. The cast and homogenized ingot was converted to plate by a series of hot working operations, including hot forging followed by hot rolling. The hot forging was performed at 1000°C and consisted of multiple forging steps with reheat to provide a squared ingot suitable for hot rolling. The squared ingot was hot rolled in multiple steps also with reheat between rolling passes to obtain a 10 mm thick plate. Subsequent heat treatment of the plates consisted of normalizing at 1150°C for 30 min followed by air cooling to near room temperature. The plate was then tempered at 700°C for 1 h followed by air cooling to room temperature. The chemistry of the NETL version of MARBN-type steel is shown in Table 1.

For tensile testing, mechanical test specimens were machined in a dog-bone geometry of 2.54 and 0.6 mm -thicknesses. Specimens were then polished using 600 grit abrasive to a uniform surface finish. Prior to tensile testing a set of specimens were exposed to a 650°C environment consisting of CO_2, 4% vol H_2O and 1% vol O_2. This manuscript will refer to this exposure environment as direct fired 4% or "DF4". The tube furnace was conditioned by heating it to 50°C for several hours under CO_2 flow. This approach was used to remove residual oxygen from the furnace tube. The furnace tube was

subsequently ramped at 200°C/h to 650°C where the oxygen and water mixture was injected into the tube furnace flow. The specimens were subjected to the DF4 condition for 1000 h, at which point the oxygen and water flow was stopped and the specimens were cooled in the furnace in flowing CO_2 to room temperature. An additional set of tensile specimens were exposed in a similar manner in vacuum at 10^{-6} torr also at 650°C for 1000 h. These specimens were used to assess thermal conditions and cycle for comparison.

The tensile specimens were weighed before and after the exposures. Tensile testing was performed on an Instron servo-electric tensile frame equipped with Bluehill analytical software. ASTM E8 was adhered to when performing tensile tests. Tensile testing was performed at room temperature, with extension rates of 0.05 mm/min until failure.

For creep testing, cylindrical specimens were employed with a gage diameter of 6.35 mm and a reduced section length of 25.4 mm. Prior to initiation of the creep test the retort tube was held at 50°C for several hours under CO_2 flow, also to remove residual oxygen from the system. The system was subsequently ramped to 650°C and a flow of 100 SCCM of gaseous CO_2 (99.999% purity) was maintained until specimen failure. A load of 207 MPa was selected for creep test comparison. An additional set of test specimens were creep tested in the retort creep frame in laboratory air.

Results and Discussion

Select tensile specimens of P91 and 347H steels were exposed to the DF4 condition for 1000 h prior to tensile testing. The mass gain under DF4 conditions is tabulated in Table 2. For the P91 steel for both section thicknesses, similar mass gain was observed. For the 347H stainless steel some spallation led to a reduction in mass for the 0.6 mm thick specimen. However, the 2.54 thick specimen had about 15% of the mass gain of P91. This suggests thicker sections of 347H alloy are more resistant to oxidation under the DF4 conditions. Mass gains in vacuum were negligible for both thicknesses of P91 and 347H steels.

Table 2. Mass gain from DF4 exposure after 1000h.

Alloy	Specimen Thickness (mm)	Mass gain (mg/cm^2)
P91	0.50	29.0
P91	2.54	28.0
347H	0.60	-6.0
347H	2.54	4.6

The tensile properties for the various steels are tabulated in Table 3. No significant change in mechanical properties was noted for vacuum exposures for both the 0.5 and 2.54 mm thicknesses of P91 steel. For P91 steel, the thin 0.5 mm thick specimen exposed to DF4 conditions failed before reaching its yield stress (YS). The designated ultimate tensile strength (UTS) in Table 3 was 336 MPa; however, as the specimen failed before yielding this value is not accurate and more appropriately termed the fracture strength. With the elongation less than 1% the specimen was severely embrittled by the exposure. The thicker, 2.54 mm thick specimen of P91 showed slight reduction in YS and UTS

while, the elongation reduced by 57% after exposure to DF4 conditions. These limited results suggest the P91 may be inadequate for use in the DF4 conditions.

Table 3. Tensile properties of various steels.

Alloy	Thickness (mm)	Exposure	0.2% Yield (MPa)	UTS (MPa)	Elongation (%)
P91	0.5	As received	570	697	11
P91	0.5	Vacuum	523	652	12
P91	0.5	DF4	---	336	0.5
P91	2.54	As received	554	698	21
P91	2.54	Vacuum	538	683	20
P91	2.54	DF4	487	665	9
347H	0.6	As received	235	670	62
347H	0.6	Vacuum	253	632	52
347H	0.6	DF4	486	642	3
347H	2.54	As received	230	661	83
347H	2.54	Vacuum	258	660	86
347H	2.54	DF4	257	661	85
MARBN	6.35	As received	825	984	24
MARBN	6.35	DF4	NT	NT	NT

Indeed, Akanda et al.[6] found that the thinner section of P91 were severely embrittled. Figure 1 shows the overview perspective of the fracture surfaces from the two thicknesses of P91 steel. Both left and right images in Figure 1 are scanning electron microscopy (SEM) backscatter electron images, showing contrast by atomic density, meaning atomically heavier phases appear brighter. From the left image in Figure 1, a darker ring (arrowed, Figure 1) is clearly visible around the periphery of the sample. This suggests an atomically lighter phase such as an oxide layer was present. The oxidation/carburization affected zone measured ~200 µm in thickness. Note: this measurement includes the growth of the oxidation zone. Akanda et al.[6] confirmed the oxide layer thickness by microprobe analysis of this region which was rich in oxygen and Cr. From the right hand side image of Figure 1, the thicker specimen did not show any severe carburization. However, the oxide layer spalled from the sample due to the forces generated during tensile testing. Using microprobe analysis, Akanda et al.[6] found only minor differences between the oxidation affected zone thicknesses for the two specimen thicknesses in P91 steel. However, an carburized zone extending approximately 0.8 mm into the 2.54 mm thick specimen was observed. The thinner sample of P91 had elevated carbon as well, but as the sample thickness was less than 0.8 mm (the depth of the carburized zone for the thicker specimen), this is to be expected.

Figure 1. Fracture surface from P91 Steel exposed to DF4 environment for 1000 h, Left) Thin specimen, Right) Thick specimen.

Elevated carbon levels are indicative of breakaway oxidation phenomena. The mechanism of breakaway oxidation is contested in the literature, however, breakaway oxidation occurs when elevated levels of carburization occur in the oxide layer, and oxide growth shifts from parabolic (diffusion limited) to linear kinetics. While Akanda et al.[6], were unable to confirm breakaway oxidation by gravimetric studies, the elevated carbon levels in the oxide from both the 0.5 mm and 2.54 mm thick P91 specimens suggests the alloy was in the beginning stages of breakaway oxidation. Note the exposures were limited to 1000 h.

For 347H mechanical properties remain relatively unchanged for all specimen thicknesses and exposure conditions with the exception of the thin specimen at 0.6 mm thickness. For the thin, 0.6 mm specimen of 347H exposed for 1000 h under DF4 conditions, the UTS remained approximately the same as the unexposed specimen. However, the YS increased by ~2X and the elongation was severely reduced. The surface hardness increased from the starting matrix hardness to a depth of 0.2 mm, suggesting coarsening of the carbides, which also likely explains the increase in YS and the reduction in elongation at fracture.

Microprobe line scans for the oxygen and carbon profiles of the two thicknesses of 347H are shown in Figure 2. For the thinner 0.60 mm specimen of 347H a clear oxidation layer was present while for the thicker 2.54 mm thick specimen no oxygen signal registered on either side of the specimen. The thinner specimen (Figure 2, left) notably had relatively more carbon uptake than the thicker specimen (Figure 2, right) of 347H. Akanda et al.[13] determined that the thin specimen formed a Fe-rich oxide layer which

likely contributed to both the increase in thickness and carbon uptake. As the carbon levels within the oxide layer for the 0.6 mm thick 347H specimen remained low (Figure 2, left), no evidence for breakaway oxidation was found. Akanda et al.[13], attributed this increase in oxidation thickness for the 0.6 mm thick 347H specimen to failure to form of a continuous chromia scale.

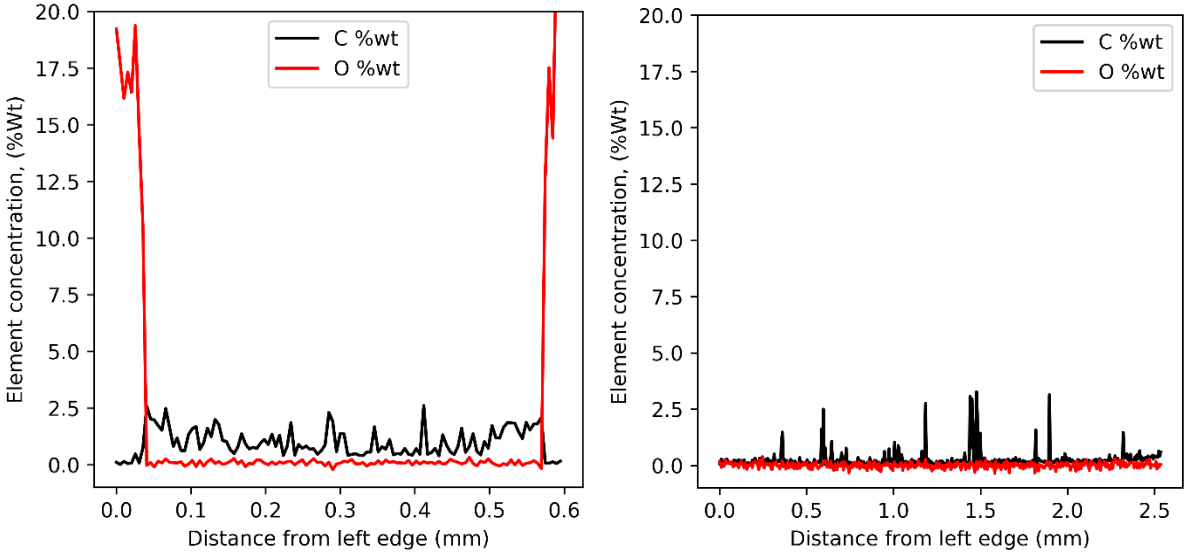

Figure 2. Microprobe line scans of oxygen and Carbon for 347H. Left: 0.60 mm thick specimen; Right: 2.54 mm thick specimen.

The fracture surface for the thinner specimen of 347H is shown in Figure 3. The images in Figure 3 are also SEM backscattered electron images. The left image in Figure 3 shows an overview of the specimen. While there is some contrast in the center of the specimen, this likely results from the inclined geometry of the fracture surface relative to the electron detector and is not related to the atomic number contrast. The right hand side image in Figure 3 shows a higher magnification area near the specimen edge. The right image in Figure 3 shows some additional contrast on the right edge of the specimen (arrowed). Akanda et al. [13] analyzed this area as oxide.

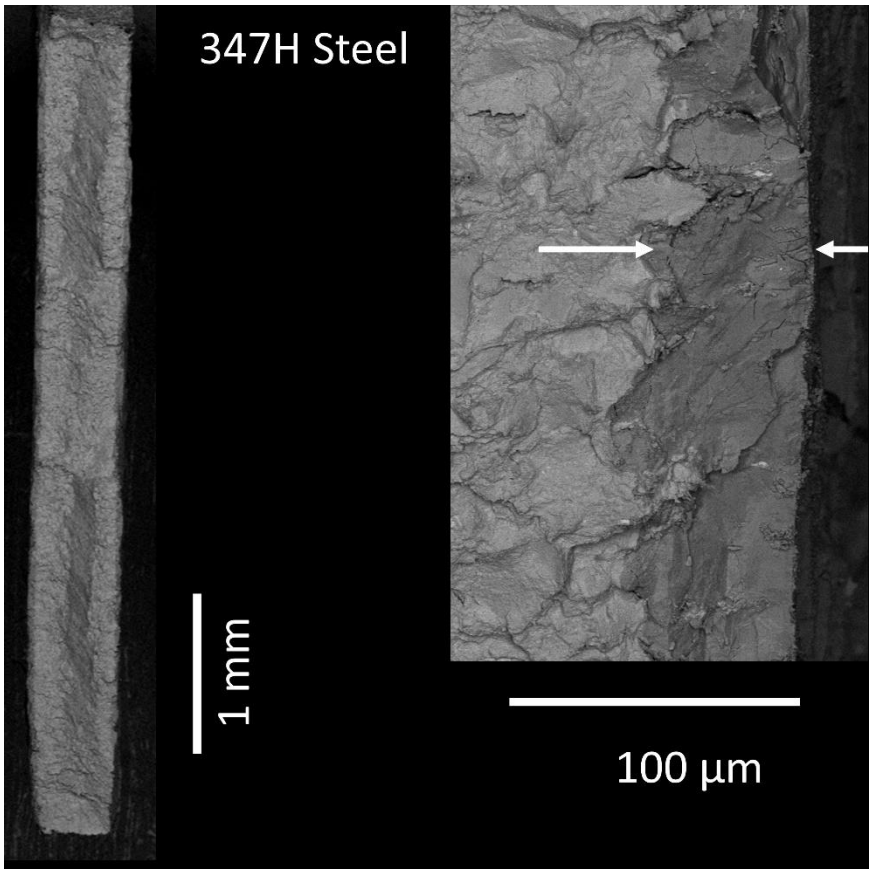

Figure 3. Fracture surface from 347H thin specimen exposed to DF4 environment. Left) Low magnification overview; Right) High magnification near specimen edge.

For the MARBN steel, the specimen was tensile tested as received in laboratory air. No DF4 exposure studies were conducted for the MARBN steel. The mechanical properties of the MARBN martensitic-ferritic steel are superior to P91 and 347H, except for the elongation, where the alloy only had 24% elongation at fracture. However, the MARBN alloy is not as corrosion resistant as 347H, as it contains ~9%Cr by weight.

Of the alloys under consideration, only the MARBN steel has been creep tested to date in gaseous CO_2. Observations for creep testing of the MARBN martensitic-ferritic steel to date include: an increase in the minimum creep rate (MCR), a severe creep life reduction in gaseous CO_2 with little to no change in elongation to failure or reduction in area at fracture. Specimens creep tested in gaseous CO_2 experienced a reduction in time to rupture of approximately 3.5X. See Table 4 for summary of testing conditions and post failure results.

Table 4. Creep properties of MARBN steel in gaseous CO_2 and air.

Alloy Designation	Test Temperature (°C)	Stress Level (MPa)	Time to Failure (h)	Elongation to Failure (%)	Reduction in Area (%)	Minimum Creep Rate (%/h)	Larson Miller Parameter, C=25
MARBN - Air	650	206.84	527	13.2	64.4	$2.21 \cdot 10^{-3}$	25586.18

MARBN - Air	650	206.84	545	12.6	69.9	$1.74 \cdot 10^{-3}$	25605.15
MARBN - CO_2	650	206.84	169	16.1	67.3	$8.20 \cdot 10^{-3}$	25129.21
MARBN - CO_2	650	206.84	140	14.7	58.3	$1.00 \cdot 10^{-2}$	25054.18

The detriment in creep life is visually represented in Figure 4 which shows creep strain as a function of creep life. The pink squares and red triangles creep tests on NETL MARBN steel conducted in air while the black circles and blue stars were identical creep tests conducted in gaseous CO_2. It is apparent that the creep tests were repeatable both under air and gaseous CO_2 conditions. Furthermore, the reduction in creep life at 650°C at 206.84 MPa was approximately 3.5X that compared to the creep tests conducted in air.

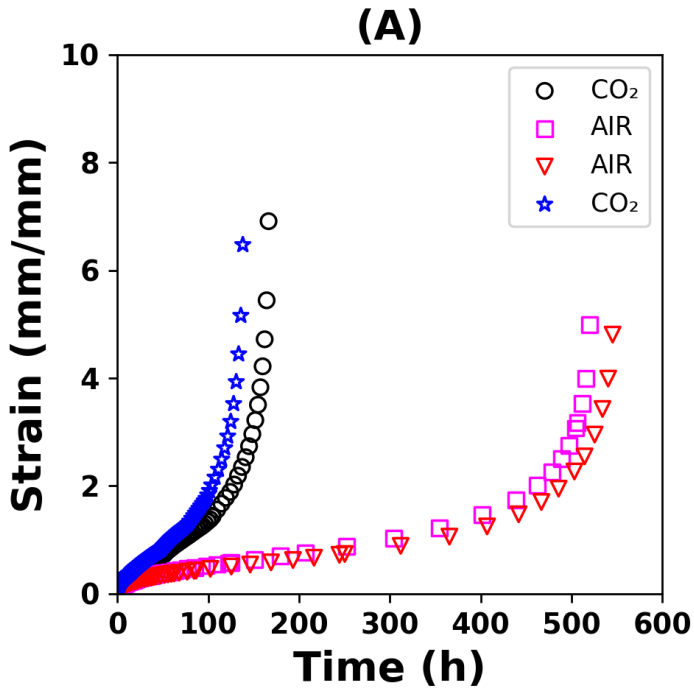

Figure 4. Strain-Time relationship for MARBN steel creep tested in air and gaseous CO_2.

Fracture surfaces show larger and deeper profile cracks from the specimens creep tested in gaseous CO_2 that for those conducted in air. Figure 5 shows the profile view of the fractured creep specimens, with the left-hand image showing the gage section and fracture for the specimen creep tested in air while the right-hand image shows similar view for the NETL MARBN specimen creep tested in gaseous CO_2. Both images are SEM backscattered electron images showing atomic number contrast. It is apparent that the base metal underneath the oxide scale is brighter. This is more pronounced on the right-hand image where the secondary cracks through the oxide layer are deeper and more frequent.

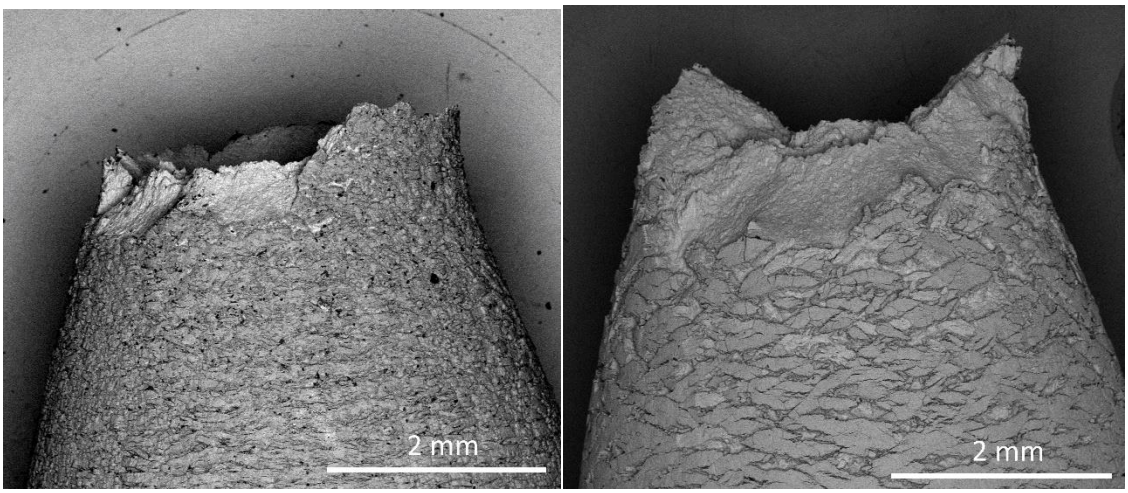

Figure 5. Profile view of fractured specimens, Left) in air, Right) in gaseous CO_2.

Rozman et al. [11] studied this material in depth. As with the P91 and 347H steels, case hardening due to carbide formation was found. It was observed that environmentally assisted cracking provided a self-sustaining accelerated cracking mechanism. The carbon tended to deplete the Cr from the matrix, thereby favoring carbides and allowing further oxygen ingress.

Creep testing 347H in gaseous CO_2 is ongoing. Specimens will be tested in air and gaseous CO_2 at 650°C at 196 MPa. Given the increase in oxidation thickness and carbon uptake in the thinner 347H specimens (see Figure 2 and 3), specimens were cut to have flat rectangular gage sections of 2.0 mm, 1.0 mm and 0.5 mm thicknesses. These experiments will examine the effect of specimen thickness under creep in gaseous CO_2. The round 6.35 mm diameter specimen of 347H failed at 882 h in air. The specimen with the 2.0 mm rectangular cross section failed at 852 h, also in air, showing very good experimental consistency for the different gage section geometries.

Conclusion

The one thing this research has shown conclusively is that care should be taken when selecting steels for service in CO_2 environments. After exposure to a mixture of CO_2 – 4% H_2O - 1% O_2 at 650°C, thin sections of both ferritic-martensitic P91 steel and austenitic 347H showed an overall loss in material behavior (either strength or ductility or both). In particular, ductility was severely reduced due to excessive carburization. In general, P91 ferritic-martensitic steel was more severely degraded under these conditions compared to 347H.

The NETL MARBN martensitic-ferritic steel, which is similar in composition to P91 but significantly stronger due to the incorporation of B and N, was creep tested in gaseous CO_2. As with the P91 the MARBN steel showed a propensity to undergo significant oxidation and carburization and failed much sooner than specimens tested identically in air. Creep testing of 347H under gaseous CO_2 is ongoing. In addition to creep testing in gaseous CO_2, the effect of specimen thickness and specimen geometry is also being investigated.

Acknowledgments

This work was performed in support of the U.S. Department of Energy's Fossil Energy Crosscutting Technology Research Program. The authors would like to thank several NETL staff for their support in these projects. Dr. Joseph Tylczak performed the tube furnace exposures. Drs. Jeff Hawk, Paul Jablonski, Martin Detrois for providing and designing MARBN material. Chris Powell performed the mechanical testing. Matthew Fortner and Christopher McKaig conducted the metallography work and Keith Collins performed a portion of the microscopy analysis.

Disclaimer

References

[1] Oleksak RP, Rouillard F. 4.14 - Materials Performance in CO2 and Supercritical CO2. In: Konings RJM, Stoller RE, editors. Comprehensive Nuclear Materials (Second Edition). Oxford: Elsevier; 2020. p. 422-51.
[2] Pint BA, Brese RG, Keiser JR. Effect of pressure on supercritical CO2compatibility of structural alloys at 750 °C. Materials and Corrosion. 2017;68:151-8.
[3] Lee HJ, Kim H, Kim SH, Jang C. Corrosion and carburization behavior of chromia-forming heat resistant alloys in a high-temperature supercritical-carbon dioxide environment. Corrosion Science. 2015;99:227-39.
[4] Lee HJ, Subramanian GO, Kim SH, Jang C. Effect of pressure on the corrosion and carburization behavior of chromia-forming heat-resistant alloys in high-temperature carbon dioxide environments. Corrosion Science. 2016;111:649-58.
[5] Brittan A, Mahaffey J, Anderson M. Corrosion and Mechanical Performance of Grade 92 Ferritic-Martensitic Steel After Exposure to Supercritical Carbon Dioxide. Metallurgical and Materials Transactions A. 2020;51:2564-72.
[6] Akanda SR, Oleksak RP, Repukaiti R, Rozman KA, Doğan ÖN. Effect of Specimen Thickness on the Degradation of Mechanical Properties of Ferritic-Martensitic P91 Steel by Direct-fired Supercritical CO2 Power Cycle Environment. Metallurgical and Materials Transactions A. 2021;52:82-93.
[7] Martin WR, McCoy HE. Effect of CO2 on the Strength and Ductility of type 304 Stainless Steel at Elevated Temperatures. Oak Ridge, Tennessee: Oak Ridge National Laboratory; 1962.
[8] McPherson, Donagla, Wakeley, Kohes, Sheriff, Dragen. High-Temperature Creep Evaluation in Carbon Dioxide Atmosphere. Chicago Illinois: Illinois Institue of Technology; 1961.
[9] Guo J, Cao T, Cheng C, Meng X, Zhao J. Effect of carburization (pyrolysis furnace tube main failure factor) on the microstructure and properties of HPNb alloy tube. Engineering Failure Analysis. 2020;115:104610.
[10] Kim SH, Cha J-H, Jang C. Corrosion and creep behavior of a Ni-base alloy in supercritical-carbon dioxide environment at 650 °C. Corrosion Science. 2020;174:108843.

[11] Rozman KA, Oleksak RP, Doğan ÖN, Detrois M, Jablonski PD, Hawk JA. Creep of MARBN-type 9Cr martensitic steel in gaseous CO2 environment. Materials Science and Engineering: A. 2021;826:141996.
[12] Jablonski PD, Hawk JA. Homogenizing Advanced Alloys: Thermodynamic and Kinetic Simulations Followed by Experimental Results. J Mater Engin Perf 2017;26:4-13.
[13] Akanda SR, Oleksak RP, Repukaiti R, Rozman KA, Doğan ÖN. Effect of thickness on degradation of austenitic 347H steel by direct-fired supercritical CO2 power cycle environment. Corrosion Science. 2021;192:109795.